

Effect of Electrochemical Bath Composition on the Preparation of Ni-W-Fe-P Amorphous Alloy

Josiane Dantas Costa¹, Mikarla Baía de Sousa¹, José Jaílson Nicácio Alves¹, Bianca de Oliveira Evaristo², Raíssa Alves Queiroga², Aureliano Xavier dos Santos², Theóphilo Moura Maciel², Ana Regina Nascimento Campos³, Renato Alexandre Costa de Santana^{3}, Shiva Prasad³*

¹ Department of Chemical Engineering, Federal University of Campina Grande, Av. Aprígio Veloso, 882, 58429-970 Campina Grande, Brazil

² Department of Mechanical Engineering, Federal University of Campina Grande, Av. Aprígio Veloso, 882, 58429-140 Campina Grande - PB, Brazil

³ Department of Biology and Chemistry, Federal University of Campina Grande, R. Olho D' Água da Bica, S. N., 58175-000 Cuité-Pb, Brazil

*E-mail: renatoacs@ufcg.edu.br

Received: 31 October 2017 / Accepted: 19 December 2017 / Published: 5 February 2018

The effect of nickel sulfate and sodium tungstate concentrations in an electrolytic bath on the process of obtaining the Ni-W-Fe-P alloy in the presence of a complexing agent and at high pH is investigated in the present work. The full 2^2 factorial planning points plus two central points are used for the development of the work. For this study, within the range of the proposed variables, the optimum concentrations found were 0.02 M nickel sulfate and 0.09 M sodium tungstate, achieving a 497 HV microhardness. The alloys obtained showed nodules and microcracks on their surfaces. It was observed that an increase in the sodium tungstate concentration in the bath favored the increase in the tungsten content, and this had a direct influence on the microhardness and corrosion resistance behavior. The best results were obtained with a tungsten content of approximately 18 at%. Values of tungsten above 22 at% in the film favored the increase in internal tension, thus promoting a greater number of microcracks, and these caused a reduction in the microhardness and corrosion resistance. All the coatings were amorphous.

Keywords: Electrodeposition, tungsten alloys, experimental planning, optimization.

1. INTRODUCTION

The process of creating and characterizing metallic coatings represents a very important part of the surface treatment industry [1]. This is because several industrial fields use metal alloys as

protective coatings in order to improve the physical, chemical and mechanical properties of the substrate, such as the wear and corrosion resistance at high temperatures [2].

There are several methods for obtaining metallic coatings, such as physical vapor deposition [3], chemical vapor deposition [4], plasma spray [5], hot dipping [6] and electrodeposition [7,8]. Among the methods cited, electrodeposition has received a great deal of attention because of its distinct advantages, such as ease of maintenance, low manufacturing cost, control of the coating thickness, ability to coat a substrate with complex geometry and ability to generate coatings with high purity [9-11]. In addition, the electrodeposition allows the control of experimental parameters such as the electrolytic composition, deposition temperature, applied current density, load to be deposited and pH of the solution. The control of these parameters favors the study of the physical and chemical characteristics of the coatings.

By using the electrodeposition process, it is possible to deposit pure metal or metal alloys formed by more than one element. The tungsten coatings obtained by electrodeposition have been increasing in use in recent years because these alloys have a high thermal stability and high hardness and are resistant to corrosion and wear [12]. These properties are excellent and render the tungsten coatings a good substitute for hard chromium (a coating that presents hexavalent chromium in its electrolytic bath, which in turn is toxic and has environmental restrictions) [13-15]. Hard chromium coatings lose their protective efficiency when subjected to high temperatures.

The direct electrodeposition of tungsten from aqueous solutions containing the tungstate is prevented by the formation of an oxide layer on the cathode, and in such a case, all the current used in the process is consumed for the evolution of hydrogen [16]. In this way, tungsten cannot be electrodeposited alone, and its reduction only occurs in the presence of an inducing metal and a complexing agent; this phenomenon is known as "induced co-deposition" as was reported by Brenner [7]. From this knowledge, some researchers have developed electrolytic baths containing other metals and verified that the electrodeposition of tungsten was successful in the presence of metals in the iron group such as Fe, Ni, Co and recently Cu [17].

The electrodeposition of Ni-W alloys has been investigated for decades [18-21], because the coatings obtained have interesting characteristics (high hardness and resistance to high temperature) for industrial applications. Some investigators have indicated that the alloys with high tungsten content showed more resistance, and for this reason, electrolytic baths containing complexing agents were developed [22]. In addition, it was verified that forming these alloys by electrodeposition is more efficient in weak acids and alkaline baths [23].

It is possible to find several reports on the electrodeposition of Fe-W alloys [24-27]. The main interest in the development of these alloys is related to their magnetic properties. Barbano et al. [28] carried out a study on Fe-W alloys and found that the coatings obtained with high percentages of W (32 wt%) presented amorphous (or nanocrystalline) structure, and this generated coatings with magnetic behavior. From these results, magnetic nanowires of Fe-W inside membranes were developed.

The tungsten binary alloys cited (Ni-W and Fe-W) may present cracks caused by internal stress when the tungsten content is too high or when the current density is high [25, 29]. Many investigators believe that the Ni-Fe-W ternary alloy can exhibit the key properties of these binary coatings while

also eliminating undesirable properties (for example, internal defects and stresses) [30, 31], especially if the ternary alloy has an amorphous structure, because this type of structure presents homogeneity and a lack of electrochemically active sites that generate coatings with low corrosion rates [32].

The factors that allow the creation of amorphous material by electrodeposition are not yet well known. However, some researchers report that the presence of metalloids such as P and B can generate amorphous coatings [33]. These elements are co-deposited with some transition metals, producing a series of defects, and this causes a distortion in the crystalline lattice that generates the amorphous character in the coating [34].

Some studies on the Ni-W-Fe ternary alloy are found in the literature [15, 30, 31, 35-37], but little has been reported about the presence of phosphorus in this alloy [38]. This work aimed to provide information on the electrodeposition of Ni-W-Fe-P coatings. Thus, the variation in sodium tungstate and nickel sulfate concentrations in the electrolytic bath was investigated to evaluate the influence of these parameters on the morphology, chemical composition and corrosion resistance of the coatings obtained.

2. EXPERIMENTAL PROCEDURE

This study began with the preparation of the electrochemical bath, which was composed of the following reagents: nickel sulfate (0.09-0.50 M), sodium tungstate (0.02-0.09 M), ferrous ammonium sulfate (0.005 M), ammonium citrate (0.50 M), ammonium sulfate (0.50 M) and boron phosphate (0.00043 M). All baths were prepared with bidistilled and deionized water. The pH of the bath was kept at a constant 8.5, which was adjusted by adding ammonium hydroxide or sulfuric acid as needed.

2.1. Experimental planning

Experimental planning and response surface methodology (RSM) are important tools to determine the optimum conditions of a process, as they allow the creation of an adequate mathematical model with the minimum number of experiments [15]. According to the literature [34, 39, 40], factorial planning involves the creation of a set of experiments in which all relevant factors are varied simultaneously. This procedure facilitates the analysis of results, since it is possible to identify the ideal conditions and factors that most influenced the results, as well as additional details, such as the existence of interactions and synergies between the factors. Due to these advantages, this tool has been widely used in recent years and can be applied in different areas of knowledge [41-46].

In the present work, this tool was used to evaluate the influence of the electrochemical bath parameters, since they were prepared following a complete factorial design (2^2) with the addition of two experiments at the central point, totaling 6 experiments per matrix. In the evaluation of the results obtained by the experimental design, the response surface and variance analysis (ANOVA) methodology were used as an auxiliary tool. The independent factors (the nickel sulfate and sodium

tungstate concentrations) were evaluated at the -1, 0 and +1 coded levels, according to Table 1. All experiments were performed in random order to avoid systematic errors.

Table 1. Actual and coded levels of the variables of factorial design 2^2 to obtain the Ni-W-Fe-P alloy

Inlet variables	Level (-1)	Level (0)	Level (+1)
Sodium tungstate (M)	0.090	0.295	0.500
Nickel sulfate (M)	0.020	0.055	0.090

2.2. Electrodeposition

The electrodeposition process was carried out in a glass cell with a capacity for 100 ml of the electrolytic bath. A copper cathode and a cylindrical platinum mesh anode were inserted in the cell. The cathode used was a copper substrate, cut into a square ($2 \times 2 \text{ cm}^2$) that was mechanically and chemically treated prior to the electroplating process. The mechanical treatment consisted of polishing with SiC sandpaper with P400, P600 and P1200. The chemical treatment consisted of immersing the electrode in a 10% NaOH solution to remove any residue, then immersing in a 1% H_2SO_4 solution to remove the oxide layer formed, and finally washing the sample with distilled water.

A potentiostat MQPG-01 from MicroChemistry was used to control the current density, which was set to 120 mA cm^{-2} . All experiments were conducted at 288 C of charge. A Princeton Applied Research model 616A electrode was used for cathodic rotation control and was held at a constant rate of 50 rpm. Electrodeposition was performed at room temperature.

2.3. Characterization of the surface and chemical composition of the Ni-W-Fe-P alloy

The morphological study of the Ni-W-Fe-P alloy was performed by Scanning Electron Microscopy (SEM) using a TESCAN VEGA 3SBH microscope. The surface images were made using 1000x magnification without the samples suffering any previous treatment, such as polishing or superficial chemical attack.

The chemical composition was determined by the energy dispersive X-ray (EDX) technique using an EDX-7000 Shimadzu X-ray dispersive energy spectrometer.

X-ray diffraction (XRD) tests were used to evaluate the microstructure of the alloy, using a Shimadzu XRD-6100 diffractometer, with Cu Ka radiation ($\lambda = 1.54 \text{ \AA}$) at 30 kV and 30 mA, a step size of 0.02 and a dwell time of 1 s. The scan range was from 30° to 60° .

Vickers microhardness tests were performed with a Shimadzu DUH-211 Ultra-micro hardness meter with a Berkovitch penetrator. For each point and test, three measurements were taken, in each sample, seven points were analyzed, and the penetrator depth was limited to $3 \mu\text{m}$ for 30 seconds.

2.4. Corrosion Testing

To evaluate the behavior of the corrosion resistance, linear potentiodynamic polarization (LPP) and electrochemical impedance spectroscopy (EIS) techniques were used. The electrochemical measurements were performed on a glass cell with a polytetrafluorethylene (Teflon®) cap composed of three electrodes: a saturated calomel electrode (SCE) that was used as the reference electrode, a platinum sheet with a surface geometric area of 9.5 cm², which was used as the auxiliary electrode, and the copper substrate coated with the Ni-W-Fe-P alloy, which was used as the working electrode. Each corrosion test was performed in 100 ml of a 0.1 M NaCl aqueous solution at room temperature (approximately 25 °C). The area of the working electrode exposed to the corrosion tests was 1 cm². The Stern-Geary equation was used to calculate the polarization resistance [47].

Initially, the samples were stabilized in open circuit potential tests with a stabilization time of 60 minutes. The LPP curves were obtained with a scanning rate of 1 mV s⁻¹ using a PGSTAT 302N potentiostat/galvanostat from Autolab connected to NOVA 1.11 software. The polarization technique was used to determine the electrochemical corrosion parameters: the corrosion potential and corrosion current density of the coatings obtained. Finally, EIS tests were carried out with the frequency ranging from 1 kHz to 4 mHz and a 0.01 V amplitude; the equipment used was the same as for the LPP measurements and was connected to NOVA 1.11 software. The equivalent circuit was simulated by the NOVA 1.11 software.

3. RESULTS AND DISCUSSION

3.1. Electrodeposition and characterization

The chemical composition analysis carried out by X-ray dispersive energy spectroscopy (EDX) tests allowed for the identification and quantification of the metals present in the alloy formed in the electrodeposition process, and the results obtained are shown in Table 2.

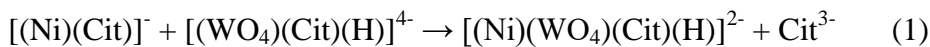
Table 2. Results of the chemical composition and microhardness of the Ni-W-Fe-P alloy

Exp.	Sodium tungstate (M)	Nickel sulfate (M)	Ni (at%)	W (at%)	Fe (at%)	P (at%)	Microhardness s (HV)
1	-1 (0.090)	1 (0.090)	81	10	8	1	483
2	1 (0.500)	1 (0.090)	73	24	2	1	544
3	-1 (0.090)	-1 (0.020)	60	18	21	1	497
4	1 (0.500)	-1 (0.020)	28	27	43	2	401
5	0 (0.295)	0 (0.055)	69	22	8	1	513
6	0 (0.295)	0 (0.055)	69	22	8	1	508

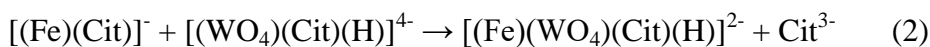
The effect of the variations in the concentrations of nickel sulfate and sodium tungstate in the electrolytic bath on the generation of the Ni-W-Fe-P coatings was evaluated. According to the data in

Table 2, it was observed that an increase in the nickel sulfate concentration in the bath increased the atomic content of nickel in the obtained coatings. For the tungsten to be reduced, it was necessary for there to be synergy with the Ni^{2+} , Co^{2+} , or Fe^{2+} ions belonging to the iron group. On the other hand, the metals in the iron group may be deposited readily in the absence of WO_4^{2-} . The present work indicated that increasing the Ni^{2+} concentration increased its deposition efficiency. However, a very high Ni^{2+} concentration in the bath results in a decrease in the percentage of tungsten in the alloy, as shown in experiment 1 of Table 2.

It has been confirmed that the reduction process is of the induced co-deposition type. Tungsten is only reduced in the presence of nickel and iron ions and requires a complexing agent to be present in the electrolytic bath. Several studies report that tungstate forms an intermediate complex, which is responsible for the displacement of the reduction potential that favors the reduction of tungsten in the alloy [48, 49]. Citrate (Cit) is the complexing agent used in most of the reported works because it favors the reduction of tungsten metal in the alloy in comparison with other complexing agents. The complex formed depends on the pH of the electrolytic bath, i.e., in the pH range between 3 and 5, the complex is $[(\text{WO}_4)(\text{Cit})(\text{H}_2)]^{3-}$, and in the pH range from 5 to 8, a gradual increase of $[(\text{WO}_4)(\text{Cit})(\text{H})]^{4-}$ occurs. The reduction of tungsten is favored in alkaline pH, so the complex $[(\text{WO}_4)(\text{Cit})(\text{H})]^{4-}$ is responsible for the increase in the reduction of tungsten in the alloy. The highest atomic content of 24 at% tungsten was obtained in this work. This content may have been limited by the presence of ammonium ions in the bath. According to Younes-Metzler et al. [22], the presence of ammonium ions in the bath improves the quality of the coating but limits the reduction of tungsten between 20-25%, which was confirmed in this work. The formation of the mixed complex can be represented by Equation 1:



It was observed that with the decrease in the nickel sulfate concentration and the increase in the tungstate concentration, the highest tungsten content and the lowest nickel content were obtained. In addition to this, an increase in the iron content in the alloy was observed at the maximum level of 43 at%. Iron can also form a mixed complex with tungsten, participating in the reduction of tungsten, according to Equation 2.



In this work, a low concentration of iron sulfate was used because of the ease in causing the reduction of the iron in relation to other metals. This type of process is called anomalous co-deposition. In this type of co-deposition, the less noble metal reduces preferentially with respect to the more noble metals [50, 51]. With the decrease in the nickel sulfate in the bath, the increase in iron ions at the electrode/electrolyte interface favors the formation of $[(\text{Fe})(\text{WO}_4)(\text{Cit})(\text{H})]^{2-}$ and reduces the formation of $[(\text{Ni})(\text{WO}_4)(\text{Cit})(\text{H})]^{2-}$. Even with a low iron sulfate concentration, there was a significant increase in the iron content in the alloy with the decrease in the nickel sulfate, thus confirming that the deposition is of the anomalous type [52].

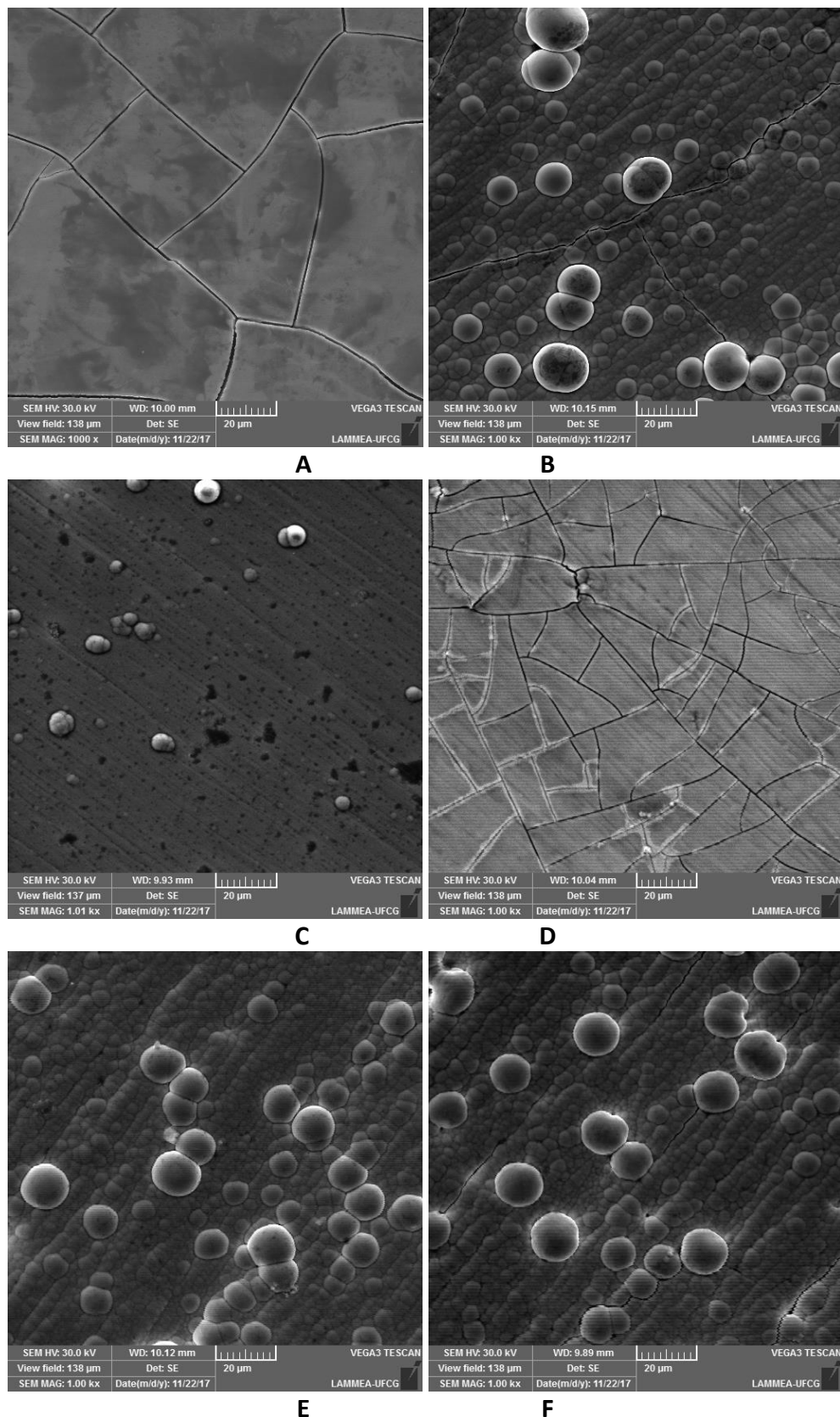


Figure 1. SEM of coatings obtained with 1000x magnification for (a) Exp. 1, (b) Exp. 2, (c) Exp. 3, (d) Exp. (4), (e) Exp. (5) and (f) Exp. (6).

It was observed that the reduction process is influenced by the induced co-deposition to reduce tungsten. At the same time, the anomalous co-deposition between nickel and iron significantly interferes in the chemical composition of the coatings obtained.

SEM images were used to evaluate the morphology of the coatings obtained. The images for each coating obtained are shown in Figure 1 (a, b, c, d, e and f). Figure 1 (a) shows that the coatings obtained presented well-defined cracks. This behavior may be associated with a higher concentration of nickel in the coating, causing an increase in its internal stress. The presence of cracks and the formation of spherical nodules with different sizes are presented in Figure 1 (b). This behavior can be associated with the increase in the tungsten content in the coating and the high amount of nickel causing an increase in its internal stress. Only the presence of nodules, but not of cracks, was observed in Figure 1 (c). A decrease in the contents of nickel and tungsten and an increase in the iron content were observed. Under these conditions, the previously observed stress did not occur in the coating. The coatings with higher contents of tungsten and iron had a higher number of micro-cracks than those obtained in other coatings in this study, as shown in Figure 1 (d). The same behavior is reported in some studies concerning the Ni-W alloy [29, 53, 54]. It can be noted from Table 2 that the deposit obtained with the highest concentration of tungsten and the lowest concentration of nickel (exp 4) had a mean composition of 43 at% iron, 28 at% nickel, 27 at% tungsten and 2 at% phosphorus and exhibited a large number of micro-cracks in the surface (Figure 1.d). This may favor a decrease in the corrosion resistance and microhardness of this coating. According to Li and Ebrahimi [55], too much of an increase in the amount of iron (above 35%) can generate internal stress and therefore more micro-cracks. Figures 1 (e) and 1 (f) showed no cracks, only nodules. Mun et al. [30] found that the addition of 8 at% of iron to the Ni-W alloy completely removed the microcracks in the coatings. Alimadadi et al. [32] performed a Ni-W alloy study and observed that the alloy with 6.7 at% W presented a large number of micro-cracks, while the alloy with 19.8 at% W presented few cracks. In the present work, uniform coatings were also obtained with the presence of circular nodules. These coatings (Exp. 3, 5 and 6) had a tungsten content of 18 and 22 at%.

The results of the Vickers microhardness measurements obtained for each experiment in this study are presented in Table 2. From these data, a response surface graph was generated to better visualize the effects of each variable (sodium tungstate concentration and nickel sulfate concentration) on the electrodeposition process (Figure 2). The coatings had a thickness between 7 and 12 μm , and to ensure that the substrate did not influence the process, an ultra-micro hardness meter was used. It is shown in Figure 2 that as the concentrations of the sodium tungstate and nickel sulfate in the bath increase, the microhardness increases. The microhardness increased with the tungsten content in the coating until the tungsten content reached 24 at%. At tungsten contents above this value, a reduction in the microhardness was observed. It was evident that the morphology of the coatings influenced the microhardness, that is, coatings that presented cracks had the lowest values of microhardness, and the experiments that did not present cracks had the highest values of microhardness. The coating of Experiment 4 was the one that had the highest tungsten content and had the highest number of cracks. Experiment 4's coating presented the highest iron content, as it had a microhardness lower than that of nickel and tungsten. This may have influenced the decrease in microhardness. Tsyntsaru et al. [25] reported that the presence of microcracks on the deposition surface may cause a decrease in

microhardness. Wu et al. [56] evaluated the microhardness of Ni-W coatings and found that an increase in tungsten content caused an increase in the microhardness for certain contents, since too much of this element caused a decrease in the microhardness.

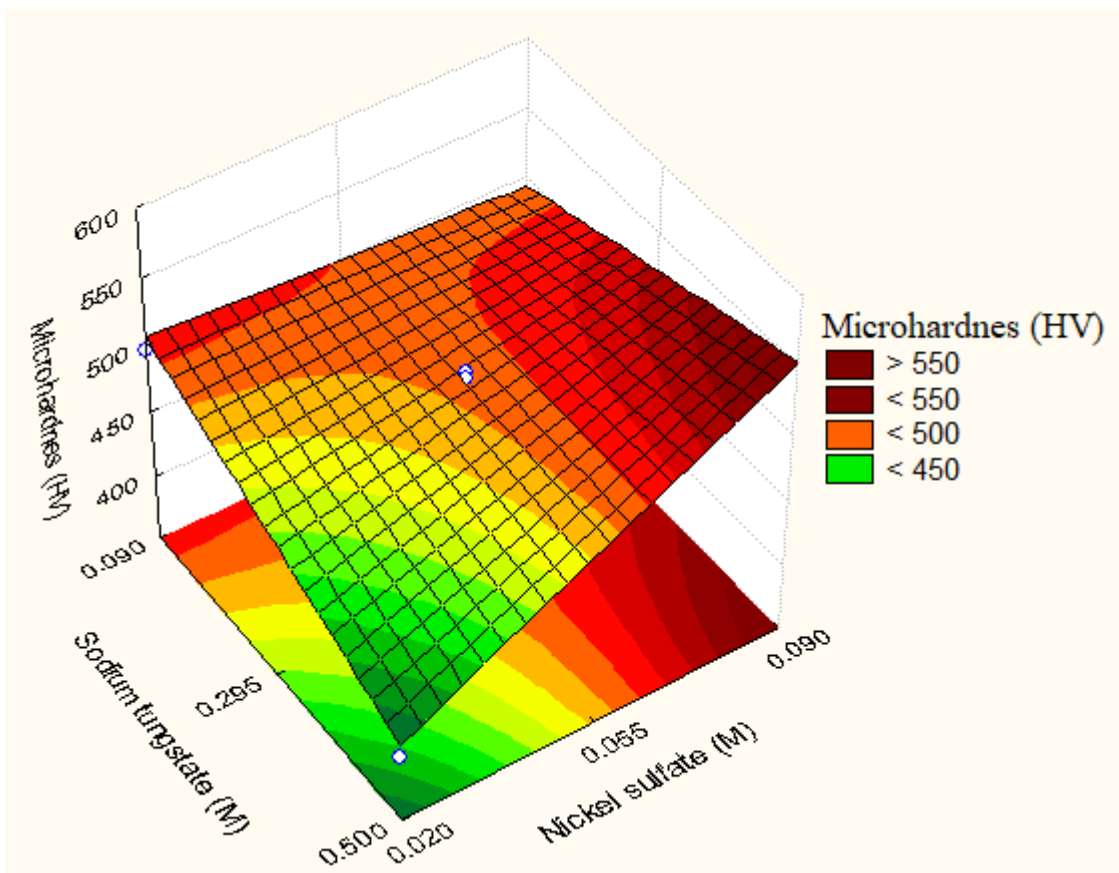


Figure 2. Response surface for the microhardness of the Ni-W-Fe-P alloy as a function of the concentration of sodium tungstate and the concentration of nickel sulfate.

X-ray diffraction tests were performed on the deposits of all the experiments. As shown in Figure 3, the deposits of all the experiments presented amorphous behavior. It was observed that with the increase in tungsten content in the alloy, the peak located at the angle of 43.5° demonstrated amorphous behavior. A similar result was observed by other researchers who worked with tungsten alloys and iron group metals [26, 48, 57-59]. According to Pisarek and collaborators [58], a binary coating with tungsten content above 20 at% exhibited amorphous behavior. Oliveira et al. [52] obtained amorphous coatings with percentages of tungsten less than 20% for ternary alloys. The deposit of Experiment 1, even though it had a tungsten content lower than the others experiments, had a broad band. This behavior may be associated with the presence of phosphorus in the alloy. Metalloids such as phosphorus and boron cause disorganization in the crystalline lattice when they are added to metal alloys, inducing the formation of amorphous coatings. The phosphorus content in the bath should be low because at high concentrations, it inhibits the reduction of tungsten in the alloy.

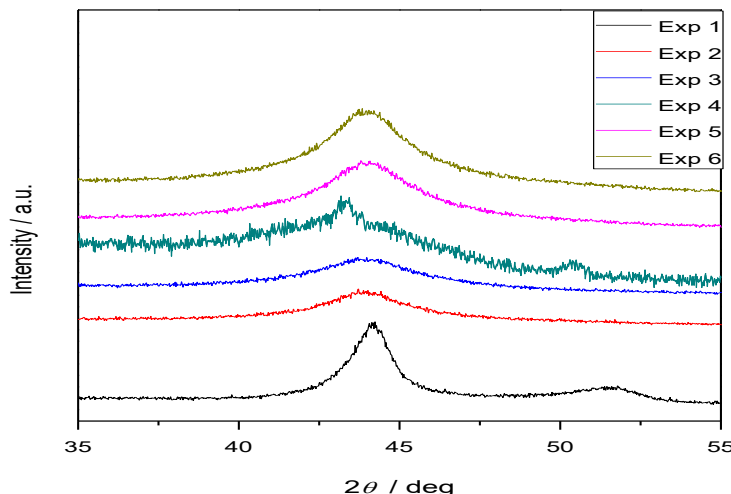


Figure 3. Standard XRD of the Ni-W-Fe-P alloy for all experiments.

3.2. Evaluation of corrosion resistance

Table 3. Electrochemical parameters obtained from the polarization curves of Ni-W-Fe-P alloy

Exp.	Sodium tungstate (M)	Nickel sulfate (M)	E _{Corr} (V)	I _{Corr} (μ A)	R _p (KΩ.cm ²)	ba (mV.dec ⁻¹)	-bc (mV.dec ⁻¹)
1	-1 (0.090)	1 (0.090)	-0.447	9.13	15.6	958	509
2	1 (0.50)0	1 (0.090)	-0.552	8.78	16.9	563	866
3	-1 (0.090)	-1 (0.020)	-0.358	1.45	30.6	143	360
4	1 (0.500)	-1 (0.020)	-0.631	6.97	9.98	677	186
5	0 (0.295)	0 (0.055)	-0.340	1.83	24.4	187	235
6	0 (0.295)	0 (0.055)	-0.353	2.03	25.3	191	275

To evaluate the influence of the concentrations of sodium tungstate and nickel sulfate on the corrosion resistance of the coatings obtained, experiments were carried out using Linear Potentiodynamic Polarization (LPP) and Electrochemical Impedance Spectroscopy (EIS) techniques.

Initially, the LPP curves were obtained and are presented in Figure 4. The LPP curves indicate that coatings with higher corrosion resistance are obtained under the conditions of experiments 3, 5 and 6, which have a more cathodic potential and higher values of polarization resistance compared to the others experiments. To quantify this information, the electrochemical parameters, such as corrosion potential (E_{Corr}), corrosion current (I_{Corr}), polarization resistance (R_p) and Tafel's slopes, were extracted from the LPP curves by extrapolating the Tafel's lines and are presented in Table 3. The corrosion current was calculated from the Stern-Geary equation:

$$ICorr = \frac{b_a \cdot b_c}{2.3(b_a + b_c)R_p} \quad (3)$$

where ba and bc represent the slopes of the anodic and cathodic Tafel's equations, respectively, and I_{Corr} represents the corrosion current.

The results extracted from the Tafel's curves are shown in Table 3. It was observed that the percentage of tungsten in the coatings obtained influenced the corrosion resistance. Coatings with tungsten percentages above 22 at% decreased the corrosion resistance.

This behavior may be associated with the increase in the internal stress, which caused the formation of microcracks, thus making the coating brittle. Sriraman *et al.* [36] reported similar behavior. Alloys with higher iron content have low values of corrosion resistance.

The coatings with tungsten percentages between 18 and 22 at% presented the best polarization resistance values. This result may be associated with the formation of amorphous coatings, without the presence of microcracks, which may favor the formation of an efficient passivation film. The decrease in the Tafel's slope values can be observed with the increase in the corrosion resistance.

The coatings from Experiments 3, 5 and 6 shown in Table 3 have nodules on their surface and do not display micro-cracks. This may favor the formation of a uniform passive layer consisting of WO_2 or WO_3 , which minimizes the interaction between the solution and the metal. The presence of the phosphorus metalloid in the coatings may favor the formation of the amorphous coating and improve the corrosion resistance of the coatings obtained.

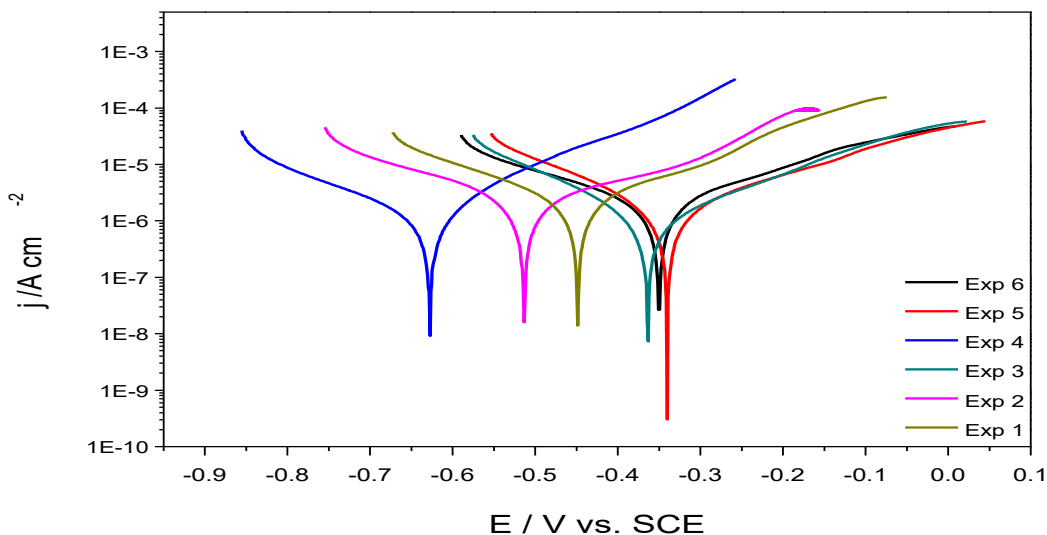


Figure 4. Linear Potentiodynamic Polarization Curves of Ni-W-Fe-P Alloy, obtained in 0.1 M NaCl.

To confirm the results obtained from the LPP curves, EIS measurements were performed on every Ni-W-Fe-P coating. All measurements were performed on open circuit potential (OCP). The EIS results are presented in the form of Nyquist diagrams (Figure 5), which confirmed the results obtained from the LPP curves. Experiment 3 resulted in the highest value of polarization resistance, while experiment 4 resulted in the lowest, similar to what was found from PPL measurements.

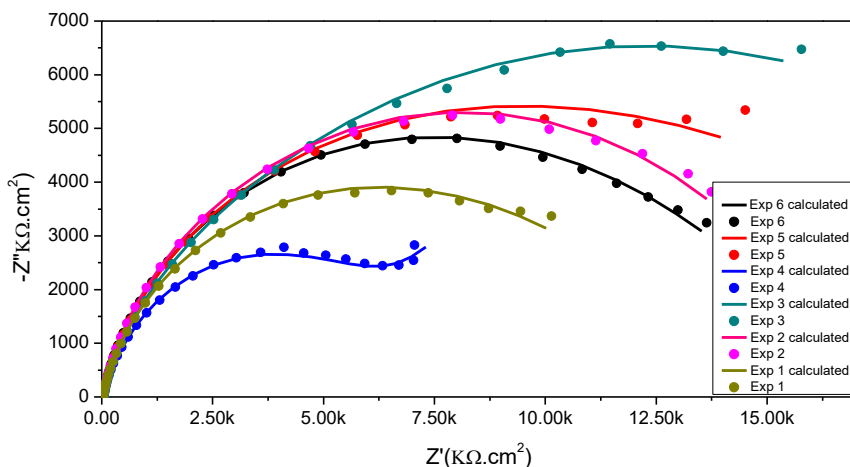


Figure 5. Nyquist diagrams for Ni-W-Fe-P alloy measured at open circuit potential.

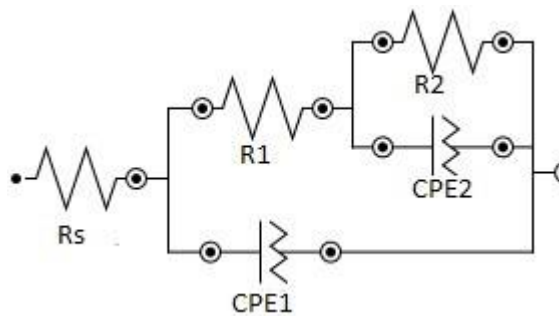


Figure 6. Equivalent electrical circuit used to adjust the experimental data of the EIS

Table 4. Adjusted parameters of the equivalent circuit for Ni-W-Fe-P alloys

Exp.	Sodium tungstate (M)	Nickel sulfate (M)	R_s ($\Omega \cdot \text{cm}^2$)	$CPE1$ ($\mu\text{F} \cdot \text{cm}^2$)	n_1	$CPE2$ ($\mu\text{F} \cdot \text{cm}^2$)	n_2	R_p ($R_1 + R_2$) ($\text{k}\Omega \cdot \text{cm}^2$)
1	-1 (0.090)	1 (0.090)	29.2	111	0.86	629	0.50	14.33
2	1 (0.500)	1 (0.090)	28.4	117	0.86	321	0.58	17.10
3	-1 (0.090)	-1 (0.020)	45.2	87	0.87	409	0.53	25.76
4	1 (0.500)	-1 (0.020)	32.6	137	0.84	832	0.41	9.96
5	0 (0.295)	0 (0.055)	35.7	103	0.87	189	0.49	18.90
6	0 (0.295)	0 (0.055)	33.9	77	0.87	246	0.48	17.98

The experimental data for the curves of the Nyquist diagram shown in Figure 5 were adjusted according to the equivalent electric circuit shown in Figure 6. In that circuit, R_s is the resistance of the solution, R_1 is the shear strength, and R_2 is the charge transfer resistance. $CPE1$ is the constant phase element of the coating, and $CPE2$ is the constant phase element of the double layer.

The polarization resistance value is the sum of R_1 and R_2 ($R_p = R_1 + R_2$). The CPE constant phase element was inserted in place of the capacitor to be able to represent the surface heterogeneity,

roughness and oxide films. Confirmation that there was a good fit can be justified by the similarity between the experimental data and the fit curves, denoted as symbols and continuous lines, respectively, in Figure 5. The values of the parameters obtained from the equivalent electric circuit are presented in Table 4.

It was observed that the resistance of the solution, R_s , does not change significantly, being in the range of 28.4 to 45.2 $\Omega \cdot \text{cm}^2$, because all the impedances were measured with the same solution (NaCl 0.1 M).

To obtain the optimal values with the smallest number of experiments, the response surface methodology (MSR) was used [42, 43]. The MSR is a set of mathematical techniques that relates the response function to be investigated to the variables of a process [60]. This part of the study aimed at evaluating the effect of sodium tungstate and nickel sulfate concentrations as well as finding optimal conditions for obtaining the most corrosion-resistant coating. After performing the experiments according to the experimental design, it is possible to obtain a response surface to evaluate and predict the effects of each variable on the process [44-46].

The experimental planning matrix is shown in Table 4. The results were adjusted to a polynomial equation using multiple linear regression. Considering that a 95% probability of confidence is satisfactory, it was possible to establish a first-order empirical model for the resistance to polarization given by Equation 4.

The experimental planning matrix is shown in Table 4. The results were adjusted to a polynomial equation using a multiple linear regression.

$$R_p = 17.4 - 3.26W - 1.07N + 4.64W*N \quad (4)$$

where W is the concentration of sodium tungstate, N is the concentration of nickel sulfate and WN is the interaction between the two variables.

Table 5. ANOVA for the resistance to polarization of Ni-W-Fe-P alloy.

Factors	Square sum	Degree of freedom	Square mean	F	P
Sodium tungstate	42.4452	1	42.44522	20.88733	0.044691
Nickel sulfate	4.6010	1	4.60103	2.26417	0.271319
Iteration	86.2112	1	86.21122	42.42461	0.022769
Error	4.0642	2	2.03210		
Total square sum	137.3217	5			

* $R^2 = 97\%$

An analysis of variance (ANOVA) of the data was performed to verify the significance of the obtained model [42, 44, 46]. It can be observed from the ANOVA that the effect of the sodium tungstate concentration and its interaction with the variation of the nickel sulfate concentration were significant for a 95% confidence level. The significance of the regression is related to the p value, i.e., the smaller the p value, the greater the significance of the model. It is considered significant when the

p value is less than 0.05. The F values were high, which confirms that the model is significant. The coefficient of determination, R^2 , was 97%. This R^2 value means that 97% of the response variables can be explained by the model and only 3% cannot be explained by the model. In this way, the first-order model can be used to evaluate the effect of the studied variables and to predict the behavior of the response variable.

The results of the ANOVA are shown in Table 5 for the resistance to polarization of the alloys.

For the model describing the polarization resistance, the analysis of the variance (Table 5) reports that the effect of the sodium tungstate concentration and its interaction with the nickel sulfate concentration were significant at the 95% confidence level, or the p-value was lower than 0.05, which was not verified for the concentration factor of nickel sulfate. The coefficient of determination (R^2) of the model was 97%, and thus, it can be concluded that the model was well-fitted to the experimental data, indicating that it is a statistically significant and highly predictive model.

The response surface of the sodium tungstate concentration vs. the concentration of the nickel sulfate is shown in Figure 7. The optimal region for the studied variables is depicted in Figure 7. With the reduction in the concentration of sodium tungstate and nickel sulfate, coatings with a high corrosion resistance are obtained. The response surface also indicates that increasing the tungstate concentration causes a decrease in the polarization resistance, as is expected from the LPP and EIS curves.

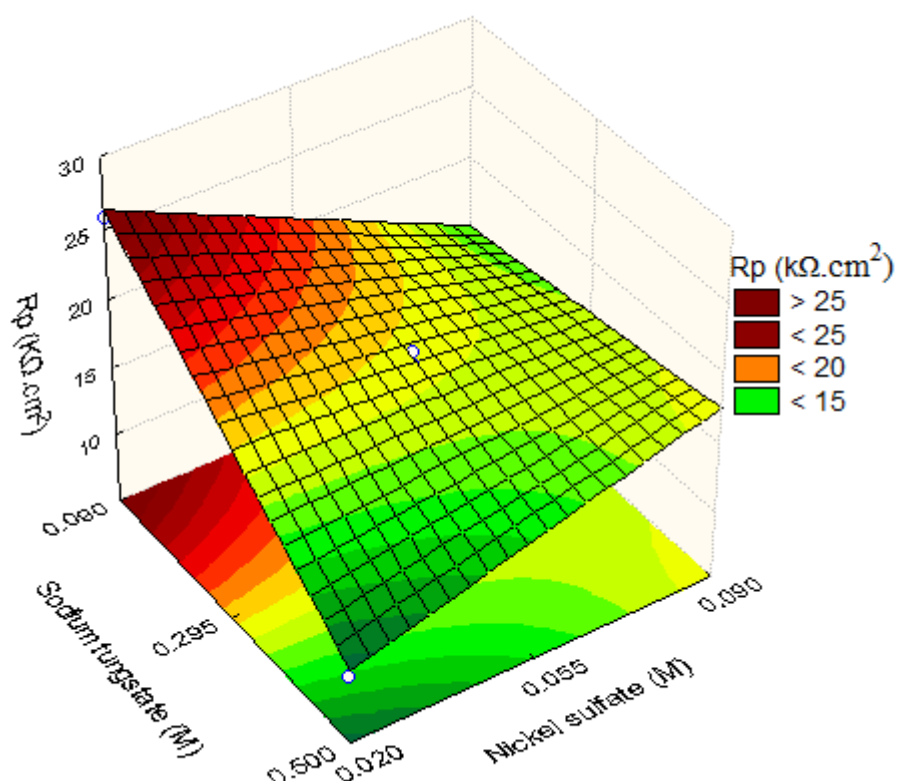


Figure 7. Response surface for the polarization resistance of the Ni-W-Fe-P alloy as a function of sodium tungstate and nickel sulfate concentrations.

Finally, it can be stated that the optimal bath concentrations are 0.02 M nickel sulfate and 0.09 M sodium tungstate. Under these conditions, a coating with a high resistance to polarization ($25.76 \text{ k}\Omega\cdot\text{cm}^2$), a uniform surface free of cracks and a high tungsten content (18 at%) were obtained. The inclusion of phosphorus in the alloy modifies its properties and favors the formation of amorphous coatings.

4. CONCLUSIONS

By the experimental study carried out in this work, it was possible to verify the following:

- The variation in sodium tungstate and nickel sulfate concentrations affected the composition of the Ni-W-Fe-P alloys. The higher nickel contents were detected in coatings obtained at higher concentrations of Ni^{2+} ions, while the higher tungsten contents were detected in coatings obtained at higher concentrations of WO_4^{2-} ions. The variation in the concentration of Ni^{2+} ions caused an inverse variation in the iron content in the deposit, whereas the phosphorus content remained constant.
- The morphological study of the alloy showed coatings with homogeneous surfaces and uniform distributions of spherical nodules, as well as coatings with microcracks. It was verified that the coatings with a higher content of tungsten presented a greater number of microcracks than those obtained in other films in this study.
- The increase in the tungsten content caused an increase in the microhardness up to a limit (24 at%). Above that, the coatings had a higher number of microcracks, and this caused a decrease in microhardness.
- The XRD results revealed that the coatings showed amorphous structure and that the increase in the tungsten content in the alloy rendered the coating more amorphous.
- The corrosive behavior was affected by the tungsten content and the number of microcracks. The polarization curves indicated that the most corrosion-resistant coatings were those with a higher tungsten content but with no microcracks on the surface.
- The electrochemical impedance data were adjusted by an equivalent electric circuit and confirmed the results obtained by the polarization curves.
- Statistical treatment of the polarization resistance data indicated that the best corrosion result was found for the lowest concentration of tungstate (0.09 M) and nickel (0.02 M).

Thus, the objective of this work was achieved, since Ni-W-Fe-P alloy coatings were successfully obtained.

References

1. F. Touyeras, J.Y. Hihn, X. Bourgoin, B. Jacques, L. Hallez, V. Branger, *Ultrason. Sonochem.* 12 (2005) 13.
2. Y. Gu, J. Liu, S. Qu, Y. Deng, X. Han, W. Hu, C. Zhong, *J. Alloys Compd.* 690 (2017) 228
3. D. M. Mattox, *Handbook of Physical Vapour Deposition (PVD) Processing: Film Formation, Adhesion, Surface Preparation and Contamination Control*, (1998) Westwood USA Noyes.

4. H.O. Pierson, *Handbook of chemical vapor deposition: principles, technology and applications*, (1999) William Andrew.
5. R. Kingswell, K.T. Scott, L.L. Wassell, *J. Therm. Spray Technol.* 2 (1993) 179.
6. Maaß, P., PeiÅ-Yker, P. (Eds.). (2011). *Handbook of hot-dip galvanization*. John Wiley & Sons.
7. A. Brenner, *Electrodeposition of Alloys: Principles and Practice*, First Edit, (1963) Academic Press Inc., New York
8. D. Landolt, *J. Electrochim. Soc.* 149 (2002) S9.
9. P. Cojocaru, L. Magagnin, E. Gómez, E. Vallés, *J. Alloys Compd.* 503 (2010) 454
10. R. López, J. Herreros, A. Garcia-Arribas, J.M. Barandiaran, M.L. Fdez-Gubieda, *J. Magn. Magn. Mater.* 196–197 (1999) 53
11. M.M. Abou-Krishna, H.M. Rageh, E.A. Matter, *Surf. Coatings Technol.* 202 (2008) 3739.
12. N. Tsyntsaru, H. Cesiulis, M. Donten, J. Sort, E. Pellicer, E.J. Podlaha-Murphy, *Surf. Eng. Appl. Electrochem.* 48 (2012) 491
13. H. Capel, P.H. Shipway, S.J. Harris, *Wear.* 255 (2003) 917
14. E.W. Broome, *Met. Finish.* 102 (2004) 42.
15. A.L.M. Oliveira, J.D. Costa, M.B. de Sousa, J.J.N. Alves, A.R.N. Campos, R.A.C. Santana, S. Prasad, *J. Alloys Compd.* 619 (2015) 697.
16. E. Lassner, W.-D. Schubert, *Tungsten: properties, chemistry, technology of the element, alloys, and chemical compounds*, Springer Science & Business Media, (1999) Viena, Austria.
17. P. Bacal, P. Indyka, Z. Stojek, M. Donten, *Electrochim. Commun.* 54 (2015) 28.
18. P.K. Gupta, A. N. Tiwari, B. K. Agrawal, *Trans. Japan Inst. Met.* 23 (1982) 320.
19. R.M. Krishnan, J.C. Kennedy, S. Jayakrishnan, S. Sriveeraraghavan, S.R. Natarajan, *Met. Finish.* 93 (1995) 33.
20. N. Eliaz, T.M. Sridhar, E. Gileadi, *Electrochim. Acta.* 50 (2005) 2893.
21. M.V.N. Vamsi, N.P. Wasekar, G. Sundararajan, *Surf. Coatings Technol.* 319 (2017) 403.
22. O. Younes, E. Gileadi, *J. Electrochim. Soc.* 149 (2002) C100.
23. M.H. Allahyazadeh, M. Aliofkhazraei, A.R. Rezvanian, V. Torabinejad, A.R. Sabour Rouhaghdam, *Surf. Coatings Technol.* 307 (2016) 978.
24. Y.D. Gamburg, E.N. Zakharov, G.E. Goryunov, *Russ. J. Electrochem.* 37 (2001) 670.
25. N. Tsyntsaru, J. Bobanova, X. Ye, H. Cesiulis, A. Dikusar, I. Prosycevas, J.-P. Celis, *Surf. Coatings Technol.* 203 (2009) 3136.
26. S. Wang, C. Zeng, Y. Ling, J. Wang, G. Xu, *Surf. Coatings Technol.* 286 (2016) 36.
27. S.A. Silkin, A. V. Gotelyak, N.I. Tsyntsaru, A.I. Dikusar, *Surf. Eng. Appl. Electrochem.* 53 (2017) 7.
28. E.P. Barbano, I.A. Carlos, E. Vallés, *Surf. Coatings Technol.* 324 (2017) 80.
29. S. Lee, M. Choi, S. Park, H. Jung, B. Yoo, *Electrochim. Acta.* 153 (2015) 225.
30. S.-J. Mun, M. Kim, T.-H. Yim, J.-H. Lee, T. Kang, *J. Electrochim. Soc.* 157 (2010) D177.
31. F. He, J. Yang, T. Lei, C. Gu, *Appl. Surf. Sci.* 253 (2007) 7591.
32. H. Alimadadi, M. Ahmadi, M. Aliofkhazraei, S.R. Younesi, *Mater. Des.* 30 (2009) 1356.
33. T. Watanabe, Y. Sakurai, Y. Hamakaw, T. Masumoto, K. Shirae, K. Suzuki, *Current topics in amorphous materials: physics and technology*¶, (1993) North-Holland.
34. R.A.C. Santana, S. Prasad, A.R.N. Campos, F.O. Araújo, G.P. Da Silva, P. de Lima-Neto, *J. Appl. Electrochem.* 36 (2006) 105.
35. F.-J. He, W. Miao, L.U. Xin, *Trans. Nonferrous Met. Soc. China.* 16 (2006) 1289.
36. K.R. Sriraman, S. Ganesh Sundara Raman, S.K. Seshadri, *Mater. Sci. Eng. A.* 460–461 (2007) 39.
37. P. Esther, C.J. Kennedy, P. Saravanan, T. Venkatachalam, *J. Non-Oxide Glas.* 1 (2009) 301.
38. J. Ahmad, K. Asami, A. Takeuchi, D. V. Louzguine, A. Inoue, *Mater. Trans.* 44 (2003) 1942.
39. K.M. Rao, G.V.R. Subbarao, *Nat. Hazards.* 60 (2012) 703.
40. R.A.C. Santana, S. Prasad, E.S. Moura, A.R.N. Campos, G.P. Silva, P. Lima-Neto, *J. Mater. Sci.* 42 (2007) 2290.

41. R. Sánchez-Tovar, M.T. Montañés, J. García-Antón, A. Guenbour, *Mater. Chem. Phys.* 133 (2012) 289.
42. B.K. Körbahti, A. Tanyolaç, *J. Hazard. Mater.* 151 (2008) 422.
43. T.G. de Lima, B.C.C.A. Rocha, A.V.C. Braga, D.C.B. do Lago, A.S. Luna, L.F. Senna, *Surf. Coatings Technol.* 276 (2015) 606.
44. M. Ibrahim Coşkun, İ.H. Karahan, Y. Yücel, *Electrochim. Acta*. 150 (2014) 46.
45. M. Poroch-Seritan, I. Cretescu, C. Cojocaru, S. Amariei, C. Suciu, *Chem. Eng. Res. Des.* 96 (2015) 138.
46. J.D. Costa, M.B. de Sousa, N.C.M.L. Fook, J.J.N. Alves, C.J. de Araújo, S. Prasad, A.R.N. Campos, R.A.C. de Santana, *Vacuum*. 133 (2016) 58.
47. G. ASTM, Standard test method for conducting potentiodynamic polarization resistance measurements, *Annu. B. ASTM Stand.* 3 (2009) 237.
48. R.A.C. Santana, S. Prasad, F.S.M. De Santana, *Eclet. Quim.* 28 (2003) 69.
49. K.A. Kumar, G.P. Kalaignan, V.S. *Appl. Surf. Sci.* 259 (2012) 231.
50. D. Gangasingh, J.B. Talbot, *J. Electrochem. Soc.* 138 (1991) 3605.
51. V. Torabinejad, M. Aliofkhazraei, S. Assareh, M.H. Allahyazadeh, A.S. Rouhaghdam, *J. Alloys Compd.* 691 (2017) 841.
52. J.A.M. Oliveira, A. de M.D. Raulino, J.L.C. Raulino, A.R.N. Campos, S. Prasad, R.A.C. de Santana, *Matéria (Rio Janeiro)*. 22 (2017).
53. L. Elias, K. Scott, A.C. Hegde, *J. Mater. Eng. Perform.* 24 (2015) 4182.
54. J. Druga, M. Kašiarová, E. Dobročka, M. Zemanová, *Trans. IMF*. 95 (2017) 39.
55. H. Li, F. Ebrahimi, *Mater. Sci. Eng. A*. 347 (2003) 93.
56. Y. Wu, D. Chang, D. Kim, S.-C. Kwon, *Surf. Coatings Technol.* 173 (2003) 259.
57. N. Fathollahzade, K. Raeissi, *Mater. Chem. Phys.* 148 (2014) 67.
58. M. Pisarek, M. Janik-Czachor, M. Donten, *Surf. Coatings Technol.* 202 (2008) 1980.
59. N. Fathollahzade, K. Raeissi, *Trans. IMF*. 94 (2016) 328.
60. R.A.C. De Santana, A.R.N Campos, S. Prasad, V.D. Leite, *Quim. Nova*, 30(2) (2007).360.

© 2018 The Authors. Published by ESG (www.electrochemsci.org). This article is an open access article distributed under the terms and conditions of the Creative Commons Attribution license (<http://creativecommons.org/licenses/by/4.0/>).